Static and Dynamic Properties of a n-$C_{100}H_{202}$ Melt from Molecular Dynamics Simulations

W. Paul*

Institut für Physik, Johannes−Gutenberg Universität, 55099 Mainz

Grant D. Smith

Department of Materials Science and Engineering and Department of Chemical and Fuels Engineering University of Utah, Salt Lake City, Utah 84112

Do Y. Yoon

IBM Research Division, Almaden Research Center, 650 Harry Road, San Jose, California 95120-6099

Received August 5, 1997[⊗]

ABSTRACT: We present in this work results from atomistic molecular dynamics simulations of a n-$C_{100}H_{202}$ melt. This work represents a first effort to simulate a fully equilibrated ensemble of chains of sufficient length to follow Gaussian chains statistics and hence Rouse-like chain dynamics, employing well-validated, realistic potentials. In order to allow full equilibration the simulations were performed at experimental densities at high temperatures (≥450 K). Here we report on the static and dynamic properties of the melt obtained from two models, a united atom and an explicit atom model, and compare these results with experiment. These comparisons allow for a quantitative evaluation of the models and provide insight into the modeled system and the influence of the level of atomistic detail considered.

I. Introduction

Both their structural simplicity and their technological importance have made *n*-alkane or polyethylene melts the subject of extensive computer simulations. Much of this effort has been devoted to the study of realistic models of these chains with varying degrees of chemical detail being represented in the potential energy functions used in the simulation.[1−16] However, no definitive potential model for PE has emerged, and various groups employ force fields yielding quite different results even for fundamental properties like chain conformations.[4] Concurrently the large computational costs for the simulation of large length and time scale properties of polymer melts have inspired work to try a quantitative modeling of these properties with coarse-grained models.[17−19] However, the consequences of various levels of approximation involved in these models on predicted properties is not yet understood.

In a series of recent papers we have reported on successful quantitative modeling of short chain *n*-alkanes[10−14] with microscopic models. In these studies an explicit atom model[11] and a united atom model[14] were used to try to quantitatively reproduce experimental data on these chain molecules. The quantitative agreement between simulations and experiment was near perfect for static quantities, and for the dynamic quantities it was within 10−20% of experiment for the explicit atom model and within 20−30% for the united atom model. This implies a comparable accuracy for the two levels of modeling in the simulations.

As was shown in ref 14 the chains that have been studied so far were too short to show Gaussian chain behavior. There was, for instance, a discrepancy between the segmental friction (defined via the Rouse model) as determined from the center of mass self-diffusion coefficient of the chains and as determined from the end-to-end vector decorrelation.[14] This discrepancy is a clear indication that the chains, which consisted only of about six statistical segments, were too short to display the Gaussian configurational statistics necessary to allow for a Rouse description of the melt chains. In ref 12 it was furthermore seen in NMR spin-lattice relaxation times (T_1) for all carbon atoms excluding the end monomers that there was a factor of 2 difference between the values for the *n*-alkane $C_{44}H_{90}$ and for a long chain polyethylene. This indicates that for the dynamics of the C−H vector reorientation C_{44} is too short to be polyethylene-like.

Experience from the computer simulation study of coarse−grained polymer models shows that chains of 10 or more statistical segments are required before the chains can be described as Gaussian coils in the melt as determined by the fact that their single chain structure factor is well approximated by the Debye function.[4,20] One could therefore expect differences in local dynamics between C_{44} and polyethylene, such as those involved with the T_1 measurements, to reflect the difference between a semiflexible chain and a Gaussian coil. It is therefore interesting to study an *n*-alkane system which can be expected to be in the Gaussian coil regime, but still short enough to exhibit Rouse-like dynamics so that reptation can be neglected. The local dynamics resulting from conformational motions of such a coil then should be closer to that of high molecular weight PE and resolve the discrepancy seen in the NMR T_1 data. Additionally it is a very challenging and fundamental question to what degree a polymer model which has been shown to quantitatively reproduce experimental static and dynamic properties adheres to the simple Rouse model generally used to analyze experiments on the dynamics of unentangled chains in the melt. We therefore resolved to study n-$C_{100}H_{202}$ melts using primarily the united atom model developed by us.[10,11,14] We will show results for two simulation temperatures, $T = 450$ K and $T = 509$ K. At the higher temperature we also performed a simulation using the explicit atom model in order to compare the results for

[⊗] Abstract published in *Advance ACS Abstracts,* December 1, 1997.

S0024-9297(97)01184-4 CCC: $14.00

the local dynamics between these two levels of modeling.

This paper is organized as follows. In section II we describe our models and the simulation techniques. Section III consists of an analysis of the static properties of the models and comparison with available experimental data. Section IV is devoted to an analysis of the local dynamics in these model systems, and section V presents our results on the large scale dynamics. In section VI we present our conclusions.

II. Models and Simulation Techniques

The united atom model is described in detail in ref 14. In this model the C−C bond lengths are constrained, and there is a bond angle potential harmonic in cos θ and a 3-fold torsion potential. The nonbonded interaction is of Lennard-Jones type, CH_2 and CH_3 having the same effective size but different energy parameters.[8,14] The explicit atom model is described in ref 11. The C−C and C−H bond lengths are constrained, the bond angle potentials are harmonic in the angle, and all torsion potentials are of the 3-fold type. The nonbonded interactions are modeled by the exponential-6 force field with different parameters for the carbon and hydrogen atoms.

All results for the dynamical properties were obtained using a Nosé−Hoover constant temperature molecular dynamics (MD) algorithm with an integration time step of 1 fs. The systems were set up for the experimental density of the respective temperature, and the volume of the simulation box was kept constant. Periodic boundary conditions were used throughout. For equilibration purposes, we used a stochastic dynamics (SD) algorithm[21] for the simulation of the united atom model using an integration time step of 10 fs. This algorithm allows for a more efficient equilibration of the model than the Nosé−Hoover type dynamics. However, due to the introduction of an external friction coefficient and stochastic forces, this algorithm cannot be used to quantitatively model the dynamical properties of the alkane system under study. The dynamic properties we obtained with this algorithm will therefore only be used to give qualitative insight into the real dynamics. At T = 450 K the results we report were obtained from a relatively short trajectory of 2 ns length preceded by an equilibration run of 1.5 ns using the SD algorithm for both. At T = 509 K we equilibrated the system even more thoroughly and performed a 3 ns equilibration run with the SD algorithm. Following this we performed another 2 ns run using the MD algorithm for further equilibration and finally performed another 9 ns run during which the static and dynamic properties were measured. The end configuration of the SD equilibration run was also used as a starting configuration for the EA simulation where another 200 ps with the MD algorithm was used to equilibrate the system locally after reinsertion of the hydrogen atoms. For calculating the static and dynamic properties in the EA model a 1.1 ns run was performed, which contains a total of 12 080 atoms. For all simulations we considered a system of 40 chains of 100 repeat units in a box at the experimental density. At 450 K the box size was L = 49.8 Å and at 509 K it was L = 50.0 Å.

III. Conformation and Structure

As a first check of the validity of our models and simulation algorithms for the description of *n*-$C_{100}H_{202}$ we look at the conformational properties of the chains. In Table 1 we present the results of a SD simulation of the united atom model at 450 K, a Nosé−Hoover MD simulation of the united atom model following equilibration with the SD algorithm at 509 K and a Nosé−Hoover MD simulation of the explicit atom model following the same SD equilibration. The average pressure in the simulation volume was $p \approx -50$ atm for the SD simulation of the UA model at 450 K, $p \approx$ 160 atm for the MD of the UA model at 509 K, and $p \approx$ 75 atm for the MD of the EA model at 509 K.

Table 1. Radius of Gyration, End-to-End Distance, Characteristic Ratio As Defined and As Comparable to SANS Experiments (See Text), and Percentage of Torsion Angles in the Trans State for $C_{100}H_{202}$ at the Indicated Temperatures[a]

	r_G [Å]	R_{EE} [Å]	C_N^{def}	C_N^{ns}	% trans
UA 450 K	16.1 ± 0.1	41 ± 1	7.2 ± 0.3	6.7 ± 0.2	61.4
UA 509 K	16.0 ± 0.1	41 ± 1	7.2 ± 0.3	6.6 ± 0.1	61.3
EA 509 K	16.0 ± 0.2	39 ± 2	6.6 ± 0.7	6.6 ± 0.3	57.6

[a] The values for the UA model at 450 K are for a SD simulation with large time step and larger discretisation errors.

Comparing the two UA simulations at 450 and 509 K there is no difference in the size of the chains within the error bars of the simulation. The EA simulation and the UA simulation also both give R_G = 16 Å at 509 K. There are two values for the characteristic ratio quoted in the table. One (C_N^{def}) is calculated following the definition as $C_N = \langle R^2 \rangle / (N-1)l^2$ where l = 1.53 Å is the C−C bond length. The experimental value for high molecular weight PE obtained from small angle neutron scattering (SANS)[22] is $C_\infty = 7.8 \pm 0.4$ at 413 K. Using standard RIS techniques[23] to correct for our smaller chain length and to extrapolate in temperature we get $C_{100} = 6.7 \pm 0.4$. Comparing this to the value of C_N^{def} we give in Table 1 we find a good agreement between simulation and experiment. For comparison with an experiment performed on C_{100} at T = 509 K we would, however, have to follow the experimental procedure, where the radius of gyration of the chain is determined from the small q behavior of the single chain structure factor. Using $6\langle R_G^2 \rangle$ instead of $\langle R^2 \rangle$ in the above formula, the result is quoted as C_N^{ns} in Table 1. This replacement is an identity in the case of infinitely long Gaussian chains, but it leads to an underestimation of the real characteristic ratio from the experimental procedure by about 8% for our chain length. This difference is in agreement with the RIS calculation of Flory for polyethylene.[23]

Figure 1 shows the single chain structure factor for neutron scattering determined from the UA simulation at 509 K in the form of a Kratky plot. For this calculation the hydrogen atoms are reinserted into a stored time sequence of UA melt configurations, their positions being determined by the positions of the adjacent carbon atoms on the chain backbone.[14] The scattering is approximated as originating from the hydrogen atoms alone. Also shown is a Debye behavior as would follow from the independently measured radius of gyration of the chains (if we use the experimental value of R_G the resulting Debye description would be almost indistinguishable from the one shown in its region of applicability). The perfect agreement at small q values is generally taken as confirmation that the $C_{100}H_{202}$ chains in the melt can be described as being Gaussian chains. In a recent work[24] it was shown that the end-to-end distance distribution function for C_{100} also can be nicely described by a Gaussian. We will see, however, in our analysis of the large scale dynamics in

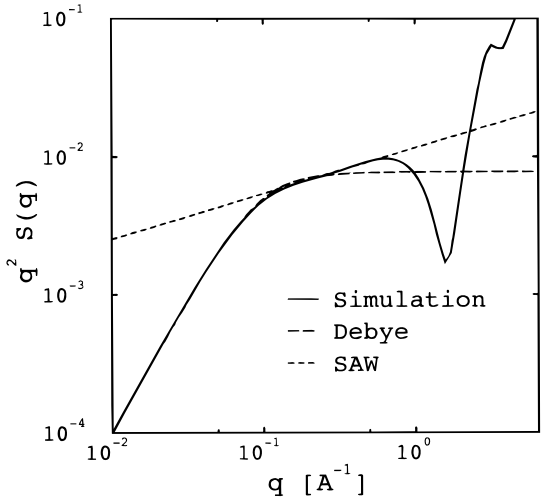

Figure 1. Kratky plot of the single chain form factor for neutron scattering (full curve) for the UA model at $T = 509$ K. The long-dashed curve is the form factor of the Debye model for a chain with a radius of gyration $R_g = 16$ Å and the short-dashed curve is the scattering behavior of the self-avoiding walk in the self-similar regime $S(q) \propto q^{-1/\nu}$.

section V that this conclusion is only valid on the largest scales of the chains. The observed scattering behavior shows a self similar regime $S(q) \propto q^{-2}$ and then deviates from this Gaussian behavior for q values larger than 0.27 Å^{-1} to follow the self-avoiding-walk (SAW) prediction $S(q) \propto q^{-1/\nu}$ with $\nu = 0.588$ up to q values where the local chemical structure of the chains dominates the scattering behavior.

To further characterize the conformational properties especially in view of possible differences between the united atom and the explicit atom description, it is instructive to look at probabilities for consecutive conformation pairs. At $T = 509$ K the values are

$$P(tt) = 0.326 \text{ (UA) vs } 0.303 \text{ (EA)}$$

$$P(tg^+ \text{ or } tg^-) = 0.574 \text{ (UA) vs } 0.545 \text{ (EA)}$$

$$P(g^+g^+ \text{ or } g^-g^-) = 0.909 \text{ (UA) vs } 0.118 \text{ (EA)}$$

$$P(g^+g^-) = 0.01 \text{ (UA) vs } 0.033 \text{ (EA)}$$

Here t is the trans-state at 180° and g^+ and g^- are the two gauche states at ±60°. There is a 2% decrease in the pair probabilities involving the trans state and a corresponding increase in the gauche probabilities going from the UA model to the EA model. There is a significant increase in the probability for g^+g^- pairs which we attribute to the slightly larger Lennard−Jones radius used for the united atom model in comparison to the combined size of the carbon and hydrogen atoms in the explicit atom model. This difference does not, however, significantly affect the overall size of the chain, as can be seen from the value of the radius of gyration in Table 1. It should be noted, however, that the g^+g^- conformer intramolecular nonbonded interactions apparently depend strongly on the atomistic detail employed in the nonbonded description. Therefore, for other polymers such as poly(ethylene oxide),[25] where intramolecular nonbonded interactions play a key role in determining energies of important conformers (unlike the high energy g^+g^- in PE), a united atom description would not be appropriate.

The fluid structure of the melt can best be described by the global static structure factor. Again the hydrogen atoms are reinserted into the UA configurations and the X-ray scattering form factors of the different atoms are explicitly taken into account. In Table 2 we compare position and width of the amorphous halo to experimental data. For both temperatures and at 509 K for both models, there is a very good agreement with the experimental data for PE for the position of the peak as well as its width. The peak position depends mostly on the density which was chosen as the correct one, but the agreement in the width of the peak shows that we are capturing the fluctuations in next-neighbor packing correctly.

Table 2. Peak Position of the Amorphous Halo and Full Width at Half-Maximum for the Case of X-ray Scattering[a]

	450 K		509 K		
	UA	exptl	UA	EA	exptl
q_{max} [Å^{-1}]	1.3	1.29	1.28	1.3	1.27
q_{FWHM} [Å^{-1}]	0.43	0.41	0.44	0.42	0.44

[a] Experimental data are from ref 26.

Overall we consider the agreement in structure and conformation between the simulations and experimental results to be very good. This finding was to be expected from our earlier results for shorter chain alkanes.[11,14]

IV. Local Dynamics

In this section we will discuss the local dynamics of the polymer chains. We will limit ourselves to a discussion of the local orientational dynamics as observed by orientational autocorrelation functions of different bond vectors in the polymer. An analysis of the translational dynamics on short time scales as observed in simulation and time of flight neutron scattering has already been reported in ref 33. We will look at the orientational autocorrelation of the unit vector along a C−H bond, the unit vector along a C−C bond, and the unit vector along the line connecting the centers of two consecutive C−C bonds in the chain, which we will denote as a chord vector. We will try to understand their behavior with respect to the torsional dynamics we observe, in particular the transitions between the trans and gauche conformers.

The torsional dynamics can be quantified in terms of the torsional autocorrelation function which is defined as

$$P(\Phi(t)) = \frac{\langle \cos(\Phi(t)) \cos(\Phi(0)) \rangle - \langle \cos(\Phi(0)) \rangle^2}{\langle \cos(\Phi(0)) \cos(\Phi(0)) \rangle - \langle \cos(\Phi(0)) \rangle^2} \quad (1)$$

The behavior of this function can be described by a stretched exponential or Kohlrausch−Williams−Watts form as discussed in detail in refs 12 and 14 and also in ref 16. We do not reproduce a figure of this function here but only give the value of the integrated autocorrelation time, which is 6 ps. This value and the autocorrelation times of the first and second Legendre polynomials of the three vectors we introduced are collected in Table 3. The integrated autocorrelation time of the torsion angles is as expected close to the mean time between torsional transitions observed in the simulation, which is 6.7 ps.

The torsional dynamics as predicted by the UA and EA models are nearly identical not only on an average time scale but also in mechanistic detail, as can be seen in Figure 2. This figure shows the probability for the next transition along a chain to occur as a function of the distance along the chain to the bond which has

Table 3. Integrated Autocorrelation Times for the Torsional Autocorrelation Function (TACF) and the First and Second Legendre Polynomial of Local Bond Vectors (See Text)

	TACF	P_1(CH)	P_1(CC)	P_1(chord)	P_2(CH)	P_2(CC)	P_2(chord)
τ_{auto}^{UA} [ps]	7 ± 1	3.3 ± 0.1	197 ± 3	288 ± 5	7.0 ± 0.1	8.3 ± 0.1	26.0 ± 0.2
τ_{auto}^{EA} [ps]	7 ± 1	4.8 ± 0.2	230 ± 30	340 ± 40	8.3 ± 0.3	14 ± 1	40 ± 2

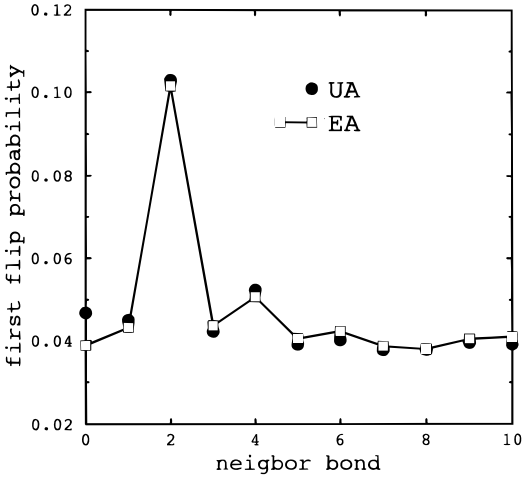

Figure 2. First flip probability after the bond at position 0 has undergone a torsional transition. Full circles are for the UA model, and open squares with full line through the data points are for the EA model.

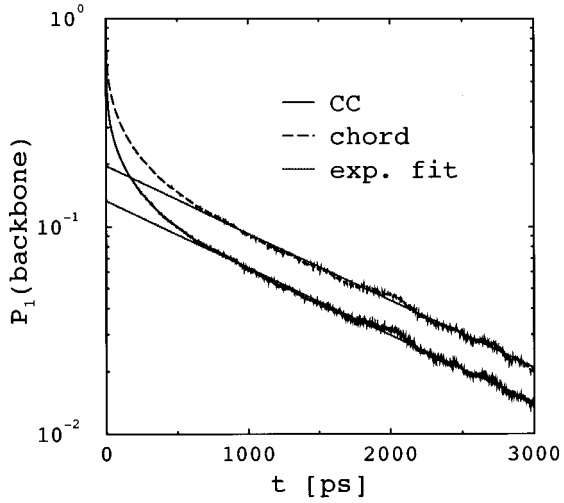

Figure 3. First Legendre polynomial of the C−C vector orientational autocorrelation function (carbon bond) and the same function for the connecting bond between centers of consecutive C−C bonds along a chain (chord) for the UA model. The straight lines are exponential fits to the data.

undergone the last transition[13] in a comparison between the UA and the EA models. There is an increased probability for second neighbor jumps (crankshaftlike motion) and also for fourth neighbor jumps, and the predictions agree between the two models. There is, however, one marked difference between the models: the UA model has an about 20% higher back jump probability, i.e., a probability for a reversal of the last transition. Another property manifesting a difference between the torsional jumps in the two models is the probability for trans−gauche versus gauche$^+$−gauche$^-$ jumps (where it is to be understood that the reversals are counted as well). These are $t - g = 0.957$ and $g - g = 0.043$ for the EA model versus $t - g = 0.915$ and $g - g = 0.085$ for the UA model.

The integrated autocorrelation times for the first Legendre polynomial $P_1 = \langle \hat{u}(t)\hat{u}(0)\rangle$ for the three vectors are 3.3 ± 0.1 ps for the C−H vector, 197 ± 3 ps for the C−C vector and 288 ± 5 ps for the chord vector for the UA model and are 20−30% larger for the EA model. The decay of the C−H vector orientational correlation function is comparable to the torsional transition rate. The other two vectors, however, which are oriented along the chain backbone, participate in the overall conformational relaxation of the chain end-to-end vector. Both vectors show a well-defined single exponential decay after an initial crossover region extending up to about 500 ps (Figure 3). The time scale of the exponential decay seen here is 1338 ps for both the chord vector and the C−C vector in the UA and about 1000 ps in the EA model. This is of the same order as the Rouse time we will discuss in the next section.

As a next quantity we will look into a characterization of the local chain dynamics via the second Legendre polynomial ($P_2 = {}^1/_2(3\langle \hat{u}(t)\hat{u}(0)\rangle^2 - 1)$) of the time displaced inner product of these vectors. Figure 4 shows all three autocorrelation functions for both the UA and the EA model. There are several features common to both models worth noting. First of all, all three relaxation functions display a two-step decay, with the second

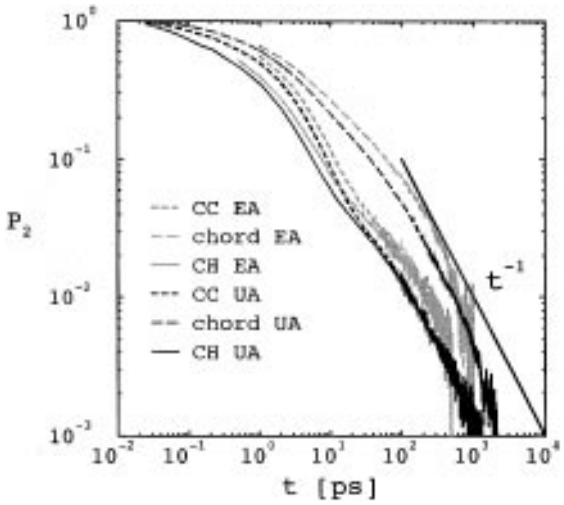

Figure 4. Second Legendre polynomial of the C−H vector, C−C vector, and chord vector orientational autocorrelation. Dark curves are for the UA model, and light curves are for the EA model. The thick line indicates a late time t^{-1} behavior according to a Rouse behavior of these functions.

process contributing only a few percent to the overall relaxation. For the chord vector this behavior is very much smeared out, since this vector averages over a larger part of the backbone, but in comparison with the other P_2 functions it is still discernible. To resolve these processes one has to be able to follow the decay over 3 orders of magnitude with high statistical accuracy as we were able to do in this simulation. We had commented on this second (long-time) process before[11,14] using a different presentation of the data, and it is possible to conclude that it contributes an appreciable amount to the overall relaxation time of the correlation functions. The ability to resolve this second process is therefore crucial for the quantitative comparison with NMR experiments we will show later. The onset of this second process is at about 10 ps, which coincides nicely

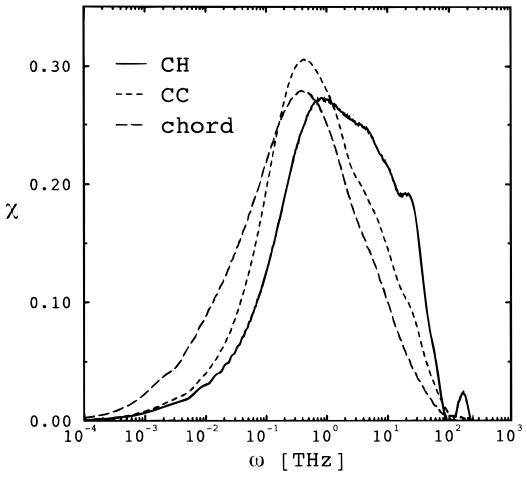

Figure 5. Susceptibility ($\omega \times$ spectral density) for the correlation functions of the UA model in Figure 4.

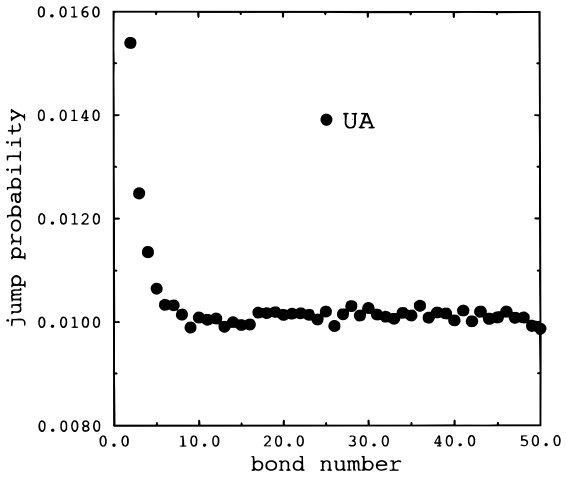

Figure 6. Torsional jump probability as a function of the backbone bond along the chain analyzed for the UA model. The data were symmetrized, and only half of the chain is shown.

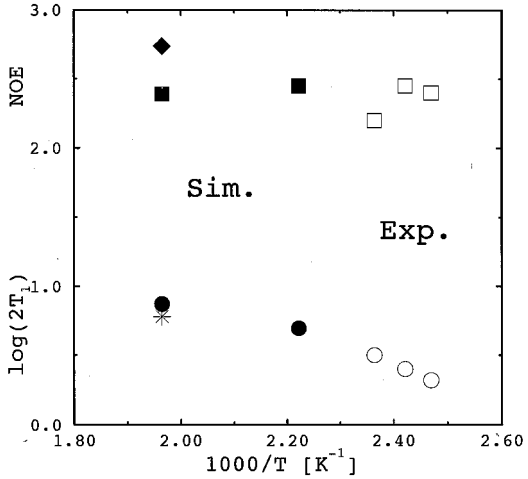

Figure 7. Spin-lattice relaxation time T_1 and nuclear Overhauser enhancement (NOE). Filled circles and squares are UA simulations at 450 (SD) and 509 K (MD), filled diamonds and stars are the EA simulation at 509 K (MD), and open symbols are experimental results on high molecular weight polyethylene. The experimental data are taken from ref 12.

with the mean time between torsional transitions. This second process therefore is the overall chain relaxation coming about by the torsional transitions. This conclusion is supported by the Rouse scaling behavior, $P_2 \propto t^{-1}$ observed for the last part of the decay for times large than 100 ps. Again one would expect a Rouse-like description of the dynamics to be applicable once enough torsional transitions have occurred, in this case about 13 per bond.

Furthermore it is interesting to note that the C−H vector and C−C vector autocorrelation functions exactly merge on the Rouse time scale. Their short-time behavior differs but there is the same amount of correlation that can only be destroyed by an overall renewal of the chain conformation. We can also note that the local vibrational and relaxational processes are about 10 times less effective in relaxing the chord vector than they are for the other two vectors. Finally, comparing the UA and the EA model, we again see our earlier findings confirmed[14] that the UA model is about 20−30% faster than the EA model.

A more comprehensive analysis of the short-time relaxation is possible when we look at the susceptibility ($\omega \times$ spectral density) connected with these relaxation functions. In Figure 5 we show a comparison of the susceptibilities for the different vectors for the UA model. The C−C and chord vector show as a main feature the relaxation peak connected with the torsional transitions, with the chord vector showing a shift of the intensity to lower frequencies as compared to the C−C vector. On the high frequency side of the peaks we only see a small shoulder indicating the torsional librations. The situation is very different for the C−H vector susceptibility. Here we see a large contribution of the torsional librations and much reduced low frequency susceptibility. In addition the C−H vector shows a contribution from the C−C−C angle vibrations, giving rise to a small peak at high frequencies (>100 THz). This motion is unable to relax the orientational correlation of the chord vector and has negligible effect on the C−C vector correlation. These larger high frequency contributions lead to the faster initial decay of the C−H vector P_2.

The second Legendre polynomial of the C−H vector orientation is also directly related to the experimentally measured spin−lattice relaxation time (T_1),[12,14] and we could show for both the UA and EA models that the experimental data on $C_{44}H_{90}$ were reproduced very well. There was, however, one puzzling experimental finding, namely that the spin−lattice relaxation times for $C_{44}H_{90}$ and for high molecular weight polyethylene were different by a factor of about 2. This finding indicates that this supposedly local quantity is influenced by chain end effects, raising the question, whether the local dynamics for the longer chain alkane we are studying in this work will be close to the PE behavior or not. In Figure 6 we show the relative rates of torsional transitions as a function of position in the chain for C_{100}. The faster transition rate near the chain-end persists only for about five to six bonds, corresponding to the statistical segment length. Hence, even for shorter chains such as C_{44} the torsional transition rate more than six bonds from the end can be expected to closely resemble that in PE. From the spectral analysis shown in Figure 5 we get our predictions for the spin−lattice relaxation time T_1 and the nuclear Overhauser enhancement (NOE)[12,14] which are shown in Figure 7 for both the UA and the EA model in comparison to the experimental data for PE.[12] Although the simulation data are only available at higher temperatures than the experimental results, we can say that the trends for both T_1 and NOE compare very nicely between simulation and experiment. The temperature dependence indicated by the

simulation data for the UA model is not to be taken quantitatively, since the data at 450 K were obtained using a stochastic dynamics algorithm and not an MD simulation. They are included here only to show the overall agreement as it was shown[10] that the SD algorithm distorts the real dynamics on large time scales. We can, however, safely conclude that the C_{100} chain behaves more like a long chain PE than the alkane C_{44}. We can speculate at this point that this is due to the fact that C_{100} is long enough to show random walk behavior in its static properties and Rouse type dynamics on large scales, but we defer a discussion of this question to the next section.

V. Large Scale Dynamics

In this section we will analyze the large-scale dynamics of the UA model and try to determine to what degree it can be understood by the predictions of the Rouse model. Let us first summarize a few of the pertinent features of the Rouse model. In this single chain model the kinetics of the chains is described as

$$\zeta \partial \vec{r}_n/\partial t = -\frac{3k_BT}{\sigma^2}(\vec{r}_{n+1} + \vec{r}_{n-1} - 2\vec{r}_n) + d\vec{W}_n(t) \quad (2)$$

Here σ is the statistical segment length of the chains, ζ is the segmental friction setting the time scale of the model and $d\vec{W}(t)$ is a Gaussian white noise with zero mean and variance $\langle dW_{n\alpha}(t) dW_{m\beta}(t')\rangle = (2k_BT\zeta)\delta_{mn}\delta_{\alpha\beta}\delta(t - t')dt$. The model can be solved analytically by a transformation to its eigenmodes,[28,29] the Rouse modes, which for a linear chain with free ends have to be defined as[30]

$$\vec{X}_p(t) = \frac{1}{N}\sum_{n=1}^{N} \cos\left(p\pi \frac{n - \frac{1}{2}}{N}\right)\vec{r}_n(t) \quad (3)$$

For the Rouse modes the model predicts

$$\langle \vec{X}_p(t)\cdot\vec{X}_p(0)\rangle = \frac{\langle R^2\rangle}{2\pi^2 p^2}\exp\left\{-p^2\frac{t}{\tau_R}\right\} \quad (4)$$

The Rouse time $\tau_R = \zeta N\langle R^2\rangle/(3\pi^2 k_BT)$ is the longest relaxation time of the chains and the Rouse modes for $p \geq 1$ are superimposed on a Fickian diffusion of the center of mass of the chains with a self-diffusion coefficient $D_N = k_BT/(\zeta N)$. Furthermore the first Legendre polynomial of the end-to-end vector autocorrelation function is given as

$$\langle \vec{R}_e(t)\cdot\vec{R}_e(0)\rangle = \langle R^2\rangle \frac{\sum_{p\ \mathrm{odd}} \frac{1}{p^2} e^{-p^2(t/\tau_r)}}{\sum_{p\ \mathrm{odd}} \frac{1}{p^2}} \quad (5)$$

The Rouse model is defined in terms of a chain of statistical segments, that is for a chain with a characteristic ratio of $C_N = 1$. A comparison with the Rouse model must therefore be based on the number of statistical segments in our chain which is approximately $^{99}/_{7} \approx 14$. As a first check of the applicability of the Rouse model to the dynamics of C_{100} chains in the melt we will analyze the self-diffusion behavior and the end-to-end vector autocorrelation, which should both be determined by the same segmental friction coefficient ζ. In Figure 8 we show the normalized end-to-end vector autocorrelation function for the UA and the EA models including a fit with the Rouse prediction of eq 5 to the UA result. If one does fits with a varying maximum number of eigenmodes, p, the result for the Rouse time, which is the only fit parameter here, converges when one reaches the number of statistical segments in the chain. The final value for the Rouse time is $\tau_R = 2090 \pm 50$ ps which leads to a segmental friction coefficient $\zeta_{\tau_R} = (1.87 \pm 0.05) \times 10^{-9}$ dyn s/cm.

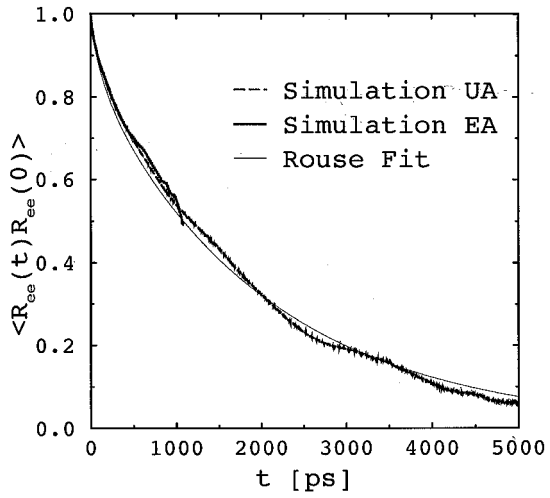

Figure 8. End-to-end vector orientational autocorrelation function. The dashed line is for the UA model, and the dotted line is for the EA model. The full curve is a fit of the Rouse prediction to the UA data using a total of 11 Rouse modes.

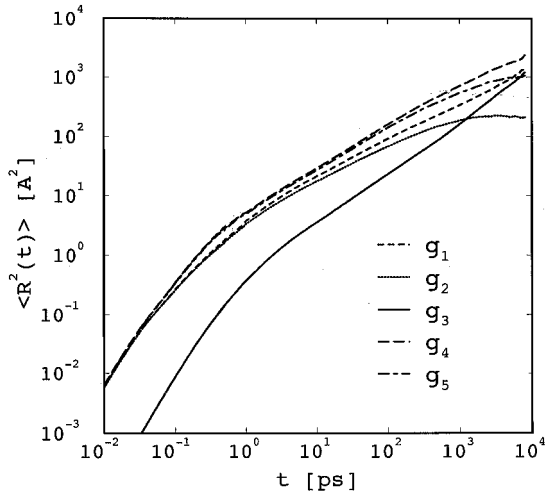

Figure 9. Various mean-square displacements (msd) in the UA model as a function of time. g_1 is the msd for the center monomers of a chain, and g_2 is the same in the center of mass reference frame. g_3 is the center of mass mean-square displacement of the chains. g_4 is the msd for the end monomers of the chains, and g_5 is the same in the center of mass reference frame.

The self-diffusion behavior of the chains is displayed in Figure 9 for the UA model. This figure shows five different mean-square displacements defined as follows: g_1 is the mean-square displacement of center monomers of the chains and g_2 is the same in the center of mass reference frame. g_4 and g_5 are the corresponding displacements for the end monomers, and g_3 is the mean-square displacement of the center of mass of the chains. The behavior of these displacements is qualitatively the same as for MD simulations of simple bead spring models[30] or, where applicable, for Monte Carlo simulations of polymer lattice models.[31] The short-time

behavior ($t \leq 1$ ps) is ballistic and out of the range of applicability of the Rouse model. The behavior of the curves for $t \geq 1$ ps is qualitatively compatible with the Rouse model predictions. Monomer mean-square displacements show a subdiffusive regime $\langle \Delta r_n^2 \rangle (t) \propto t^{1/2}$ (in the Rouse model) before crossing over to free diffusion for $t \geq \tau_R$ (g_1 and g_4) or leveling off to a plateau when measured in the center of mass reference frame (g_2 and g_5). The subdiffusive exponents one can observe are usually slightly larger than $^1/_2$, but this could be attributed to crossover effects, since the regime of validity where this subdiffusional behavior is predicted, $k_B T/(\zeta\sigma^2) \ll t \ll \tau_R$, is usually rather small. There is, however, one pronounced difference to the Rouse model predictions for times smaller than the Rouse time. The center of mass diffusion of the chains does not show Fickian behavior, but rather a subdiffusive behavior $g_3 \propto t^{0.83}$. This is again in agreement with findings of simulations of coarse grained polymer models[30−32] be they MD or MC simulations. The exponent for dense melts is always around 0.8 and does not seem to depend on chain length or temperature. For times larger than the Rouse time the center of mass self-diffusion crosses over to Fickian behavior, and one can read of a self diffusion coefficient as $D_N = \lim_{t\to\infty} g_3(t)/(6t) = (2.6 \pm 0.1) \times 10^{-6}$ cm^2/s. This value gives a segmental friction coefficient $\zeta = (1.97 \pm 0.08) \times 10^{-9}$ dyn s/cm which compares very nicely with the one obtained from the end-to-end vector reorientation. From this one can conclude that the translational and rotational diffusion coefficients of C_{100} in the melt are describable by the Rouse model. The value for the self-diffusion coefficient can also be compared to experimental results. Pearson et al.[34,35] reported on measurements of the self diffusion coefficient of a series of *n*-alkanes and polyethylene of varying molecular weight at $T = 448$ K. Their substance PW1000[34] has a degree of polymerization of about 90 and a measured self-diffusion coefficient at 448 K of $D = 1.4 \times 10^{-6}$ cm^2/s. Using the Rouse prediction to correct for the molecular weight difference and their result for the temperature dependence of the segmental friction as obtained from an analysis of this C_{90} system, $\zeta = 2.3 \times 10^{-11}$ dyn s/cm exp{1326/(T − 149)}, we would estimate an experimental value for the self-diffusion coefficient of C_{100} at 509 K of $D = 2.7 \times 10^{-6}$ cm^2/s which is in excellent agreement with our result. This agreement can also be confirmed by a comparison with neutron spin echo data on C_{100} which will be reported on in a separate publication.[36]

The global dynamics of a $C_{100}H_{202}$ melt at 500 K has also been analyzed in a recent large scale simulation employing a different and not optimized united atom force field.[15] These authors fitted a superposition of two exponentials to the end-to-end vector autocorrelation getting a total integrated autocorrelation time of $\tau_{int}^B = 1940$ ps. The integrated autocorrelation time for the Rouse model formula of eq 5 is given as

$$\tau_{int} = \tau_R \frac{\sum_{p\ \mathrm{odd}} p^{-4}}{\sum_{p\ \mathrm{odd}} p^{-2}} \qquad (6)$$

For our case the sums have to be extended up to $p = 11$ giving $\tau_{int} = 0.851\tau_R = 1778$ ps. The 10% difference between the predictions of the two models can be considered good agreement. Unfortunately the authors of ref 15 do not give the value for the center of mass self-diffusion coefficient of the chains nor do they compare it to the experimental value, but they analyze

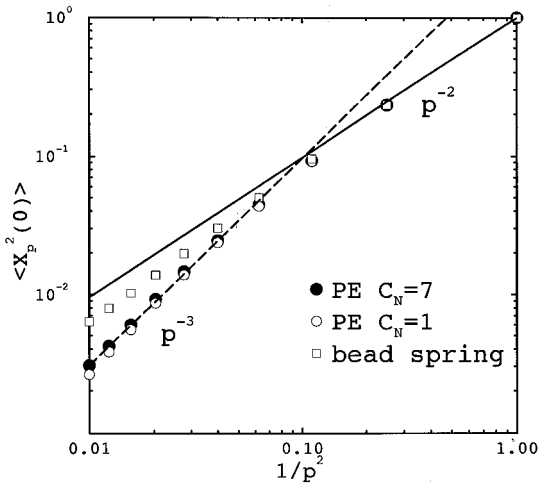

Figure 10. Squared amplitudes of the Rouse modes as a function of the predicted scaling variable p^{-2} of the Rouse model. Full circles are PE with every seventh monomer used for the calculation of the modes; open circles are PE with every monomer considered. Open squares are for a bead spring model.[30] All data sets are normalized to amplitude 1 for $p = 1$. The full line is the predicted Rouse behavior, and the dashed line is a fit to the modes $p = 4$ to $p = 10$ for PE yielding a p^{-3} behavior.

their measured mean square displacements in terms of typical relaxation times introduced in ref 31. These are defined as

$$g_1(\tau_1) = \langle R_G^2 \rangle$$

$$g_2(\tau_2) = \frac{2}{3}\langle R_G^2 \rangle$$

$$g_3(\tau_3) = g_2(\tau_3)$$

$$g_5(\tau_4) = \langle R_G^2 \rangle \qquad (7)$$

Their values are $\tau_1 = 2.3$ ns, $\tau_2 = 4.8$ ns, $\tau_3 = 2.8$ ns, and $\tau_4 = 0.75$ ns. These can be compared to the following values we obtain for our UA model: $\tau_1 = 0.61$ ns, $\tau_2 = 0.75$ ns, $\tau_3 = 1.24$ ns, and $\tau_4 = 0.49$ ns. Here we see not only very large quantitative differences between the two models but also a significant qualitative difference: we find $\tau_4 \leq \tau_1 \leq \tau_2 \leq \tau_3$, which is the same as in ref 31 in contrast to the ordering observed in ref 15. The ideal Rouse model (which assumes large N) would predict $\tau_4 \ll \tau_2 \leq \tau_1 \ll \tau_3$ with a difference of 20% between τ_1 and τ_2.[31] With the exception of an interchange of τ_2 and τ_1, which are very close in value, we see this behavior in our simulation. In ref 15 the relative magnitudes of τ_1, τ_2, and τ_3 differ very much from the Rouse model predictions. Considering the close agreement between the Rouse times as determined from the end-to-end vector relaxation, the values they quote for these typical times are also not understandable, since for the Rouse model the largest of them, τ_3, has a value of $^3/_4\tau_R$.

Let us next have a closer look at the internal modes, with their dynamics on time scales smaller than the Rouse time. As a first prediction we want to check the static scaling $\langle X_p^2(0) \rangle \propto 1/p^2$. Figure 10 shows the amplitudes of the Rouse modes for the UA model as a function of the expected scaling variable. The two data sets for polyethylene (PE) included in the figure were obtained by using only the position of every seventh monomer on the chain ($C_N = 7$), i.e., going along the

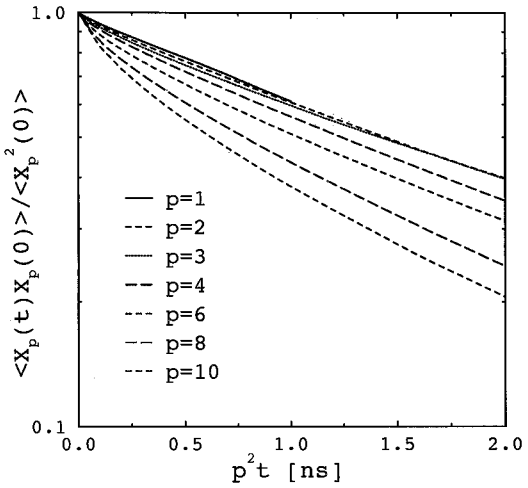

Figure 11. Dynamic scaling plot for the Rouse modes as a function of the predicted scaling variable p^2t. The mode numbers are denoted in the legend. Scaling is observed for modes $p = 1$ to $p = 3$ in a limited time window.

chain in steps of a statistical segment length, or using every monomer ($C_N = 1$) respectively. The data set denoted as bead spring is for the model of ref 30, and all three sets are normalized so that the $p = 1$ amplitude is 1. The two ways of calculating the Rouse modes for PE agree as long as the modes still follow the Rouse scaling prediction, which is at most up to $p = 3$. The higher modes systematically deviate from the Rouse prediction, seemingly following a p^{-3} behavior for the PE chains and some behavior between p^{-2} and p^{-3} for the bead spring model. The chain length analyzed for the bead spring model gives rise to a comparable number of statistical segments per chain and shows the same degree of compatibility with the Rouse model prediction. Taking into account that a mode p corresponds to the largest scale eigenmode of a chain of N'/p statistical segments, if N' was the number of statistical segments in the original chain, we see deviations for $N'/p \leq 5$. We would attribute this behavior to the fact that there are systematic deviations from the asymptotic random walk scaling, when the walk has too few statistical segments. Therefore we are probing here into the semiflexible regime of the chain conformations leading to the systematic deviations observed. However, the static cross correlation between different modes p and q is zero within the error bars of the simulation, making the Rouse modes still good eigenmodes for a dynamic analysis.

When we now look at the dynamics of the Rouse modes, we observe a comparable degree of agreement with the Rouse model as for the amplitudes. Figure 11 shows a semilogarithmic plot of the normalized mode autocorrelation for the UA model as a function of the supposed scaling variable p^2t for several selected modes. Modes $p = 2$ and $p = 3$ scale over the whole displayed time window which is roughly $(2/p^2)\tau_R$. The largest scale Rouse mode ($p = 1$) follows the scaling only up to $^3/_4\tau_R$, then displays a crossover behavior with a faster than exponential decay and, finally, for times much larger than τ_R, shows a single exponential decay again. Fits to the common scaling regime of modes $p = 1$ to $p = 3$ again lead to the same Rouse time as obtained from the autocorrelation of the end-to-end vector. The modes $p = 4$ and larger show increasingly large deviations from the Rouse scaling and also from single exponential decay. The intrinsic time scale of these modes decreases faster than p^{-2} with the mode number; the decay is, however, not compatible with a single exponential decay with time scales scaling as p^{-3} as observed in the amplitude scaling. The deviation from single exponential decay is furthermore not restricted to the modes not obeying the Rouse scaling. The modes $p = 1$, $p = 2$, and $p = 3$ also deviate from single exponential behavior in their seemingly scaling region $t \leq 1500$ ps. The deviation is rather small and increasing with the mode number. The mode decays are single exponential only asymptotically, when the chains reach the free diffusion limit ($t \geq \tau_R$). These findings again are not specific to the model of PE we study here but can be found qualitatively similar in a coarse-grained bead spring model.

The overall picture emerging for the validity of the Rouse model is that even for a chain of length close to $N_e = 138$,[37] like we are studying here, the model is at most applicable to a few largest scale eigenmodes. The translational and rotational diffusion coefficients, as obtained from the chain center of mass self-diffusion and the end-to-end vector relaxation, can be consistently described by a single intrinsic segmental friction, but these are predictions on time scales larger than the Rouse time. Due to the almost Gaussian statistics of the chain conformations, the dynamics of the chains can be analyzed in terms of the Rouse modes as eigenmodes; there are, however, systematic deviations from the predictions of the Rouse model for the behavior of these modes. These deviations can be either traced to the fact that the local conformations of the chains deviate from random walk statistics or to the fact that the chains are not freely diffusing on time scales smaller than the Rouse time due to residual interactions with the surrounding chains in the melt, which are not taken into account in the Rouse model. For chains shorter than those we look at here, the deviations due to the non-Gaussian behavior will increase, as observed in ref 14, and for longer chains the deviations due to the residual interactions with the other chains will increase, leading to reptation behavior. Consequently there may be a very small range of chain lengths where the Rouse model is at least approximately correct in its description of the internal relaxation of the chains.

VI. Conclusions

We have presented extensive molecular dynamics simulations for the *n*-alkane system $C_{100}H_{202}$. We mostly studied a united atom representation of this polymeric system and performed a comparative study for an all or explicit atom model where computationally feasible. The results for the static properties, i.e., conformation of the chains and structure of the melt, are in excellent agreement with experimental findings.

For the long time dynamics we find a very good agreement with the experimentally determined self-diffusion coefficient of the chains. A more detailed comparison with the large scale dynamics as determined by neutron spin echo experiments will be presented in a separate work.

Although the Rouse model is able to describe the translational and rotational diffusion of the chains consistently, we find systematic deviations from the Rouse model predictions in the static and dynamic behavior of the internal modes of the chains.

For the dynamics on the local scale we studied several quantities (torsional autocorrelation function; first and second Legendre polynomial of C−H, C−C, and chord vectors). We could show for the second Legendre

polynomial that the decorrelation proceeds via a two-step decay, the first being due to local vibrations and librations and the second being connected to the overall relaxation of the chain conformation coming about by the torsional transitions.

Spin−lattice relaxation time and nuclear Overhauser enhancement obtainable from the C−H vector analysis are in good qualitative agreement with the behavior experimentally seen for high molecular weight polyethylene at lower temperatures. The difference to the results obtained from simulation and experiment for n-$C_{44}H_{90}$ melts shows that the C_{100}-system is closer to the long chain limit and has at most very small residual end-effects as compared with the high molecular weight system.

All these results are furthermore in good qualitative and quantitative agreement between the united atom and the explicit atom model.

Acknowledgment. W.P. thanks IBM Germany for providing the IBM World Trade visiting scientist fellowship during which this work was started. G.D.S. acknowledges support by the SFB262 during a visit to Mainz. A generous grant of computer time at the computer center of the University of Mainz is also gratefully acknowledged.

References and Notes

(1) Ryckaert, J. P.; Bellemans, A. *Chem. Phys. Lett* **1975**, *30*, 123; *Discuss. Faraday Soc.* **1978**, *66*, 95.
(2) Vacatello, M.; Avitabile, G.; Corradini, P.; Tuzi, A. *J. Chem. Phys.* **1980**, *73*, 548.
(3) Rigby, D.; Roe, R. Y. *J. Chem. Phys.* **1988**, *89*, 5280; Takeuchi, H.; Roe, R. Y. *J. Chem. Phys.* **1991**, *94*, 7446.
(4) Bachnagel, J.; Binder, K.; Paul, W.; Laso, M.; Suter, U. W.; Batoulis, I.; Jilge, W.; Bürger, T. *J. Chem. Phys.* **1991**, *95*, 6014.
(5) Winkler, R. G.; Ludovice, P. J.; Yoon, D. Y.; Morawitz, H. *J. Chem. Phys.* **1991**, *95*, 4709.
(6) Toxvaerd, S. *J. Chem. Phys.* **1990**, *93*, 4290. Padilla, P.; Toxvaerd, S. *J. Chem. Phys.* **1991**, *94*, 5650.
(7) Krishna Pant, P. V.; Han, J.; Smith, G. D.; Boyd, R. H. *Macromolecules* **1992**, *21*, 200.
(8) Siepmann, J. I.; Karaborni, S.; Smit, B. *Nature* **1993**, *365*, 330.
(9) Krishna Pant, P. V.; Boyd, R. H. *Macromolecules* **1992**, *25*, 494.
(10) Yoon, D. Y.; Smith, G. D.; Matsuda, T. *J. Chem. Phys.* **1993**, *98*, 10037.
(11) Smith, G. D.; Yoon, D. Y. *J. Chem. Phys.* **1994**, *100*, 649.
(12) Smith, G. D.; Yoon, D. Y.; Zhu, W.; Ediger, M. *Macromolecules* **1994**, *27*, 5563.
(13) Smith, G. D.; Yoon D. Y.; Jaffe, R. L. *Macromolecules* **1995**, *28*, 5897.
(14) Paul, W.; Smith, G. D.; Yoon, D. Y. *J. Chem. Phys.* **1995**, *103*, 1702.
(15) Brown, D.; Clarke, J. H. R.; Okuda, M.; Yamazaki, T. *J. Chem. Phys.* **1996**, *104*, 2078; **1994**, *100*, 6011.
(16) Mondello, M.; Grest, G. S. *J. Chem. Phys.* **1995**, *103*, 7156. Mondello, M.; Grest, G. S.; Garcia, A. R.; Silbernagel, B. G. *J. Chem. Phys.* **1996**, *105*, 5208.
(17) Tries, V.; Paul, W.; Baschnagel, J.; Binder, K. *J. Chem. Phys.* **1997**, *106*, 738.
(18) Rapold, R. F.; Mattice, W. L. *Macromolecules* **1996**, *29*, 2457. Cho, J. H.; Mattice, W. L. *Macromolecules* **1997**, *30*, 637.
(19) Chang, X. Y.; Freed, K. F. *J. Chem. Phys.* **1996**, *104*, 3092. Guenza, M.; Freed, K. F. *J. Chem. Phys.* **1996**, *105*, 3823.
(20) Paul, W.; Binder, K.; Heermann, D. W.; Kremer, K. *J. Phys. 2* **1991**, *1*, 37.
(21) Paul, W.; Yoon, D. Y. *Phys. Rev. E* **1995**, *92*, 2076.
(22) Horton, J. C.; Squires, G. L.; Boothroyd, A. T.; Fetters, L. J.; Rennie, R. J.; Glinka, C. J.; Robinson, R. A. *Macromolecules* **1989**, *22*, 681.
(23) Flory, P. J. *Statistical Mechanics of Chain Molecules*; Hanser: Munich, Germany, 1988.
(24) Han, J.; Jaffe, R. L.; Yoon, D. Y. Preprint.
(25) Smith, G. D.; Jaffe, R. L.; Yoon, D. Y. *J. Chem. Phys.* **1993**, *97*, 12752.
(26) Ovchinnikov, Y. K; Antipov, E. M.; Markova, G. S.; Bakeev, N. F. *Makromol. Chem.* **1976**, *177*, 1567.
(27) Nosé, S. *J. Chem. Phys.* **1984**, *81*, 511. Hoover, W. G. *Phys. Rev. A* **1985**, *31*, 1695.
(28) Rouse, P. E. *J. Chem. Phys.* **1953**, *21*, 1272.
(29) Doi, M.; Edwards, S. F. *The Theory of Polymer Dynamics*; Oxford University Press: New York. 1988.
(30) Kopf, A.; Dünweg, B.; Paul, W. *J. Chem. Phys.*, submitted for publication.
(31) Paul, W.; Binder, K.; Heermann, D. W.; Kremer, K. *J. Chem. Phys.* **1991**, *95*, 7726.
(32) Kremer, K.; Grest, G. S. *J. Chem. Phys.* **1990**, *92*, 5057.
(33) Smith, G. D.; Paul, W.; Yoon, D. Y.; Zirkel, A.; Hendricks, J.; Richter, D.; Schober, H. *J. Chem. Phys.*, to be published.
(34) Pearson, D. S.; Ver Strate, G.; von Meerwall, E.; Schilling, F. C. *Macromolecules* **1987**, *20*, 1133.
(35) Pearson, D. S.; Fetters, L. J.; Greassley, W. W.; Ver Strate, G.; von Meerwall, E. *Macromolecules* **1994**, *27*, 711.
(36) Paul, W.; Smith, G. D.; Yoon, D. Y.; Richter, D.; Zirkel, A.; Rathgeber, S.; Farago, B. Manuscript in preparation.
(37) Richter, D.; Willner, L.; Zirkel, A.; Farago, B.; Fetters, L. J.; Huang, J. S. *Macromolecules* **1994**, *27*, 7437.

MA971184D